minerals

MDPI

Article

Micro- and Nanotexture and Genesis of Ball Clays in the Lower Cretaceous (SE Iberian Range, NE Spain)

Blanca Bauluz *, María José Mayayo, Elisa Laita and Alfonso Yuste

IUCA-Departamento de Ciencias de la Tierra, Universidad de Zaragoza, Pedro Cerbuna 12, 50009 Zaragoza, Spain; mayayo@unizar.es (M.J.M.); laita@unizar.es (E.L.); alfon@unizar.es (A.Y.)
* Correspondence: bauluz@unizar.es

Abstract: Ball clay deposits in the SE of the Iberian Range (NE Iberian Peninsula) consist of Albian clays and siltstones with greyish and blackish colors, interbedded with subbituminous coals. The ball clays are nowadays mined for the manufacture of white color ceramics. The mineralogy of these deposits consists mainly of kaolinite, illitic phases, and quartz. The euhedral to sub-euhedral morphology of the kaolinites suggests their in-situ origin. The anhedral morphology of the illites and the presence of frayed illites suggest a detrital origin. At the micro-scale, authigenic kaolinite booklets are observed filling pores and forming mica/kaolinite intergrowths, in which the kaolinite grows between the cleavage sheets of pre-existing detrital mica. At nanometer scale, illite/smectite (IS) phases are detected forming interlayers with mica and kaolinite, and evidence of the replacement of mica by kaolinite is observed. The matrix consists of defective illite and kaolinite, and random mixed layers of kaolinite-I/S (Kln-IS), illite-I/S (Ilt-IS), and I/S-smectite (IS-S). The textures of illite and the presence of different types of mixed layers suggest that the expandable phases and kaolinite are products of mica alteration. The effectivity of the alteration was probably a consequence of the low pH that occurred in the environment due to the presence of abundant organic- and acidic- rich fluids.

Keywords: ball clays; electron microscopy; kaolinite; Iberian range

Citation: Bauluz, B.; Mayayo, M.J.; Laita, E.; Yuste, A. Micro- and Nanotexture and Genesis of Ball Clays in the Lower Cretaceous (SE Iberian Range, NE Spain). *Minerals* **2021**, *11*, 1339. https://doi.org/10.3390/min11121339

Academic Editors: Ana I. Ruiz and Jaime Cuevas Rodríguez

Received: 30 October 2021
Accepted: 26 November 2021
Published: 29 November 2021

1. Introduction

Plastic ball clays are commonly composed of kaolinite (25%–80%), illite and mica (10%–30%), and fine-grained quartz, and sometimes illite/smectite (IS) mixed-layered minerals also occur. Organic matter—up to 4%—is also typical in these clays and a low content of coloring oxides (Fe_2O_3 and TiO_2) is a common feature. Each of these components have a specific function in the technological process [1]). The term "ball clay" is probably derived from early English mining practices, in which the clay was cut on the floors of open pits, producing approximately 25 cm cubes or "balls" weighing about 15–17 kg [1].

The ceramic properties of plastic ball clays depend on the content of the clay minerals but also on the crystallinity of the kaolinite and illite. These features influence the grain size distribution and the specific Brunauer–Emmett–Teller (BET) surface area of the clays. Plastic ball clays commonly contain large amounts of grains of <1 μm (50%–90%), and even <0.22 μm (25%–40%). The grain size of clay is, in general, inversely proportional to the specific surface area and plasticity [2].

Plastic ball clays for porcelain and refractory production have the largest qualitative variability among applied raw materials [3]. Their characteristics have to be appropriate to ensure good molding properties and mechanical strength. The presence of kaolinite promotes mullite crystallization, whereas the presence of illite and smectite influences vitreous phase formation and promotes good densification of the ceramic body during firing [4,5].

Although several studies of the composition and ceramic properties of ball clays have been published [6–11], we found a lack of research characterizing the micro- and

nanotexture of these types of clays. This information is relevant since it controls their properties and therefore their uses; deeper knowledge of these characteristics is essential to infer their genesis.

This study focuses on the Albian kaolinite-rich clay deposits associated with coal deposits located in the Southern Iberian Range (NE Spain), which can be considered ball clays in the sense of Wilson, 1998 [1]. Previously, the mineralogy of these rocks was characterized in various areas of the Oliete basin by Bauluz et al., 2008 [12] (Figure 1), indicating the abundance and distribution of the kaolinite and illite contents. This study revealed the detrital origin of the kaolinites forming the fine matrix of the clays and silts. In contrast, the higher porosity of the sandstones, according to their observations, enhanced kaolinite recrystallization during early diagenesis. The high contents of kaolin minerals in these Albian sedimentary deposits, the organic matter contents, the low iron and titanium content, and the lack of carbonates make them suitable to be actively mined nowadays for the manufacture of ceramics. The coal levels were mined, until very recently, for energetic purposes.

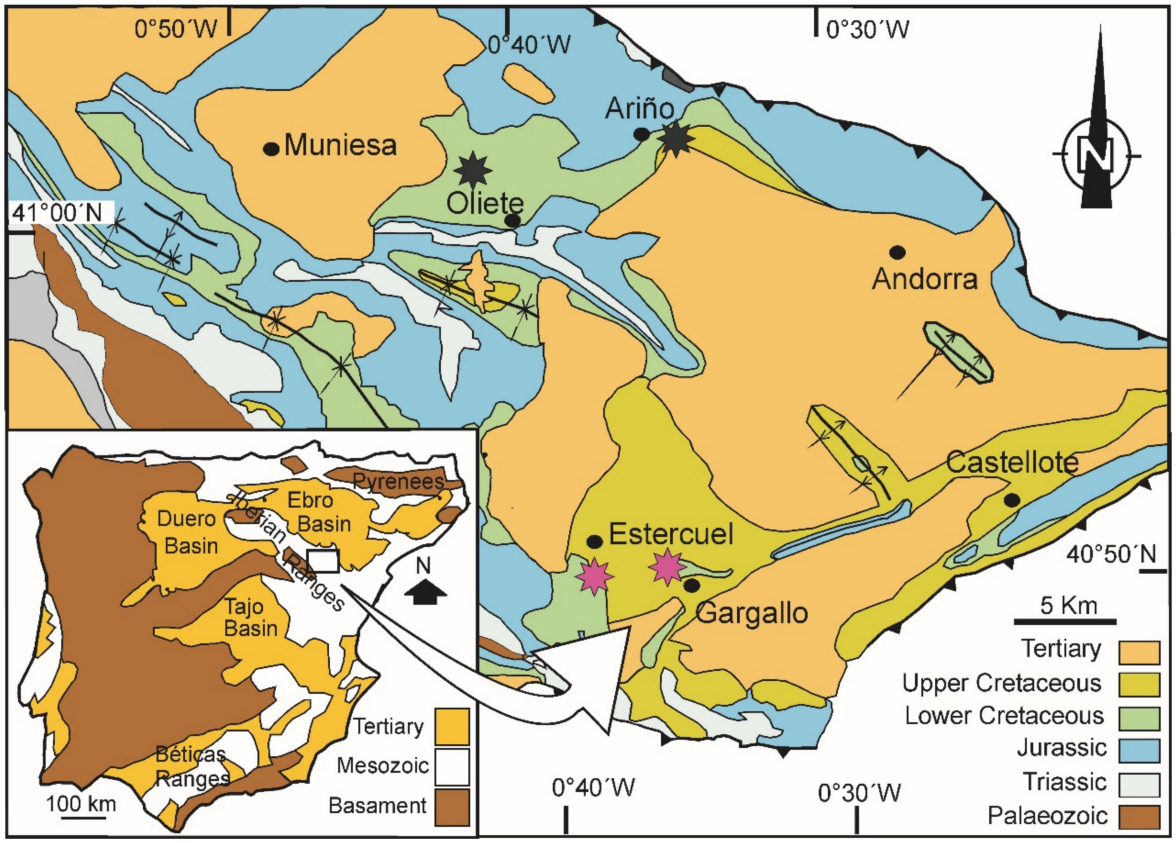

Figure 1. Ball clay deposits located and studied in the Iberian Range (Oliete Basin, NE Iberian Peninsula (blue stars: Bauluz et al., (2008) [12], red stars: this study)).

In light of the high industrial interest that these clays have for ceramic manufacture, this study has a double objective: to characterize their micro- and nanotextures using high-resolution techniques, and then to infer the formation conditions of these clays.

2. Geological Information

The ball clay deposits of NE Spain are located in the Oliete-Ariño, Utrillas-Aliaga, and Castellote basins in the SE of the Iberian Range (Oliete Basin, NE Iberian Peninsula) (Figure 1). These deposits form the Escucha and Utrillas Formations (Albian, Lower Cretaceous) and consist mostly of clays and silts with greyish and blackish colors depending on

the organic matter content; these lithologies are interbedded with significant subbituminous coal levels.

At the beginning of the lower Albian, the sedimentation in these areas was typical of a coastal marine environment, but it then evolved into a mudflat environment with freshwater swamp plains. The environmental and climatic conditions were appropriate for the formation of peat deposits containing pristine plant parts, decayed plants, decay products, and even charcoal [13].

3. Materials and Methods

Bauluz et al., (2008) mainly studied the Escucha Formation and the lower part of the Utrillas Formation in the area of Ariño-Oliete. In this research the study has been extended to the Gargallo-Estercuel zone [12].

The mineralogy of 41 claystones and siltstones that correspond to Estercuel-Gargallo (n = 41) were sampled in the middle and upper members of the Escucha Formation and analyzed by X-ray diffraction (XRD). Differentiation between claystone and silstone was made on the basis of mineralogical composition deduced by XRD. The quartz contents in siltstones is higher than 45%. These studies were carried out on randomly oriented powder mounts and oriented <2 μm fractions separated by centrifugation. Air-dried and ethylene-glycol oriented samples were analyzed to detect any expandable components. A Philips PW1729 diffractometer (Philips, Amsterdam, The Netherlands) with Cu-Kα radiation was used. For semi-quantitative estimation of the mineralogical concentrations, the intensity factors of [14,15] were applied. The XRD data were stored as computer files with the XPowderX software (version 2017.01.02) [16]. In order to characterize the clay minerals, values of kaolinite and illite crystallinity were measured on the 7 Å and 10 Å peaks, respectively, both in air-dried (AO) and ethylene (EG) oriented samples. In order to check for the presence/absence of halloysite the formamide treatment described by [17] was applied.

Following XRD, selected samples (n = 18) from the Ariño-Oliete and Gargallo-Estercuel subbasins were analyzed by field emission scanning electron microscopy (FESEM), using secondary electron (SE), backscattered electron (BSE), and energy-dispersive X-ray (EDS) analysis to obtain textural and chemical information. The observations were performed using a Carl Zeiss microscope. The accelerating voltage was 15 kV with an Iprobe of 100 pA for BSE, and it was 5 kV with an Iprobe of 100 pA for SE. Rock fragments were used for SE imaging in order to observe the morphology of the phases, and thin sections were used for BSE imaging with the aim of getting compositional images. All samples were coated with carbon for BSE and SE imaging and for EDS analysis.

Selected samples (n = 6) were also analyzed by transmission electron microscopy (TEM). The preparation of samples for TEM observation followed two different procedures.

3.1. Impregnation with London Resin White (LRW) Resin and Ion Thinning

Samples selected for microstructural analysis were prepared using a method modified from [18], as described by [19]. The method involves a multi-step exchange of the sample material with ethanol (99.9%) and LRW under refrigeration. The aim of the impregnation is to preserve the texture and the permanent expansion of smectite interlayers for TEM observation. The cured samples were cut perpendicular to the bedding, and an ordinary thin section was then prepared using a diamond saw, with oil as the lubricant to shape the samples. Sticky wax was used as an adhesive to bond the sample and the thin section glass. Several 3 mm copper rings with a hole 1 mm in diameter were glued with an epoxy resin to the areas selected for further study. After drying for 24 h, the rings were removed by heating the thin section. The rings were cleaned and ion-thinned to a suitable thickness for TEM study in a Gatan Duo ion mill (SAI, Universidad de Zaragoza, Zaragoza, Spain). The initial conditions for the ion thinning were 12°, 5 kV, and 5 mA until the first hole opened; then there was an intermediate stage with 8°, 4 kV and 5 mA; this was followed by a final stage with 5°, 3 kV, and 5 mA. The ion-milled samples were observed using a

Tecnai F30 TEM operated at 300 kV. A through-focus series of images were obtained from 1000 Å underfocus to 1000 Å overfocus, in part to obtain optimum contrast for IS ordering (overfocus) following the procedure described by [20–22]. Selected area electron diffraction (SAED) patterns were also taken from the clay-rich areas. The nomenclature proposed by [23] is used for the illite-smectite mixed-layers identified by TEM.

3.2. Particle Dispersion

Powders of the natural samples were prepared using carbon-coated Cu grids. The powder was dispersed in ultra-pure ethanol and immersed in the ultrasonic bath for 15 s. This preparation disperses individual grains of minerals onto the grid surface. The aim of this preparation is to observe by TEM the morphology of the clays and to identify them using EDS analysis.

The chemical composition of the samples were analyzed in Actlabs Laboratoires (Ancaster, Ontario, Canada). Contents in SiO_2, Al_2O_3, TiO_2, Fe_2O_3(t), K_2O and Na_2O were analyzed by X-Ray Fluorescence (XRF).

4. Results

4.1. Mineralogy (XRD Studies)

According to the XRD study, these rocks consist of quartz, kaolinite, and illite, with accessory feldspars (<5%). Calcite is only present at the bottom of the sections; the rest of the levels do not have carbonates (Figure 2). The relative proportions of each phase vary in the different lithologies. Usually, the kaolinite contents in the <2 μm fraction range from 30% to 60%, and usually its contents are higher than those of illite, the mean value of the Kln/Ilt ratio being 1.5 (Figure S1). The treatment used to check the presence of halloysite gave a negative result.

Both kaolinite and illite show variable crystallinity values. In the case of Kln, the values range from 0.36 to 0.74 in AO samples and from 0.37 to 0.72 in EG samples. This parameter in illites varies from 0.21 to 0.70 in AO and from 0.28 to 0.68 in EG. In several cases, the values are larger in EG-treated samples than in the corresponding non-treated samples, as Figure 3 shows. This is mainly observed in kaolinites but there are also some examples in illites. It is a consequence of the presence of an expandable component, probably smectite-type layers in some kaolinites and illites.

4.2. Morphology of the Clays (FESEM/SE and TEM Images)

Under FESEM, the particles of kaolinite are shown to be subhedral to euhedral nanometer-size plates and with hexagonal (or pseudohexagonal) morphologies, as Figure 4A,C show. Occasionally, halloysite tubes are observed, with sizes around 600 nm in length and 70 nm nm in thickness (Figure 4B,D). TEM images reveal the central hole parallel to the b axis of the halloysite crystal (Figure 4D). This characteristic morphology of halloysite tubes is a consequence of the layer rolling caused by the dimensional misfit between the octahedral and tetrahedral sheets and weak interlayer bonding. Halloysite was not detected by XRD, probably due to its low proportions in the samples.

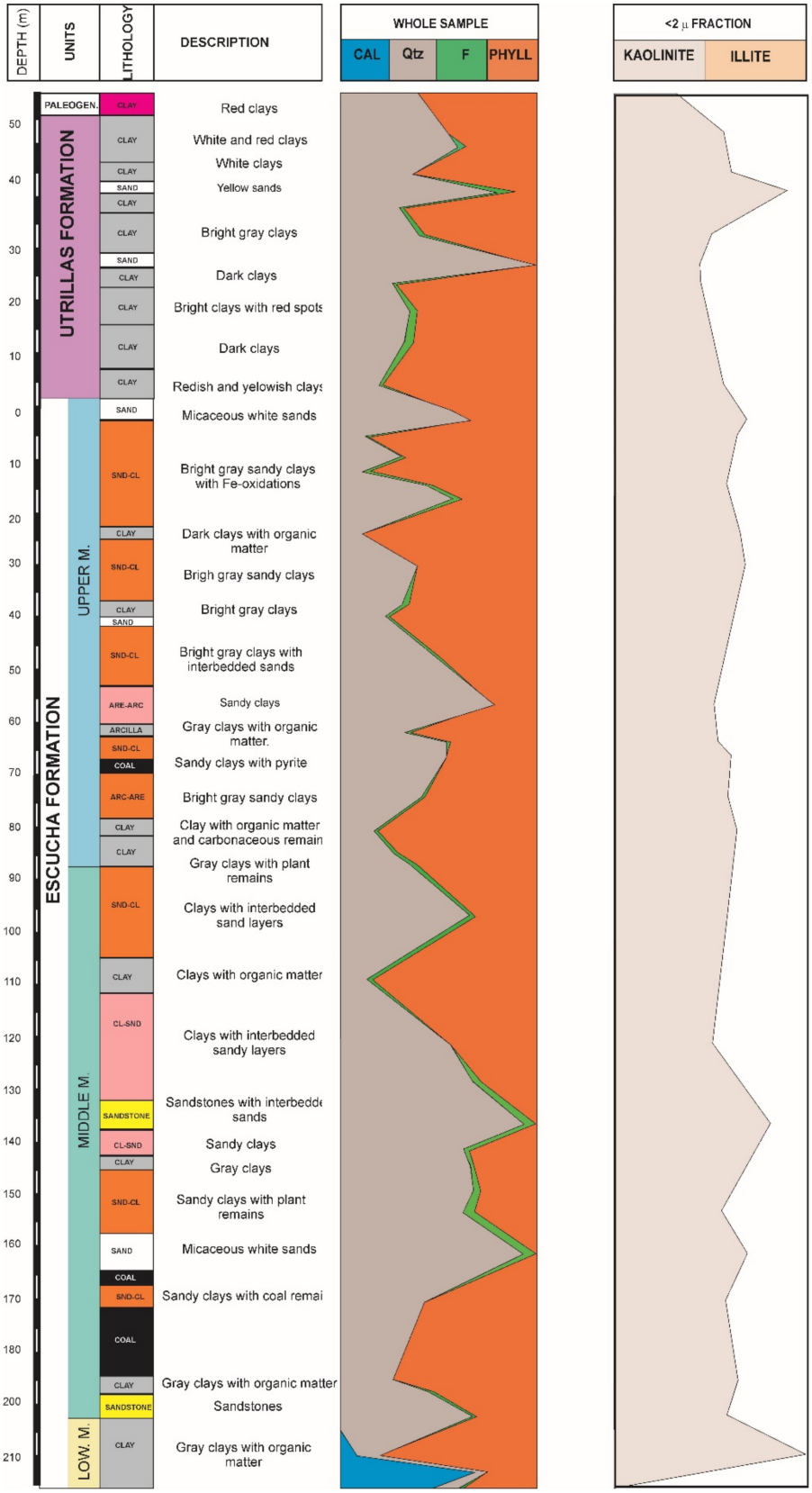

Figure 2. Representative section of the Escucha Formation and the start of the Utrillas Formation (Estercuel-Gargallo subbasin) showing lithologies and mineralogy (XRD) of both the whole sample and the less than 2 μm fraction. Cal = calcite, Qtz = quartz, F = feldspars, Phyll = phyllosilicates.

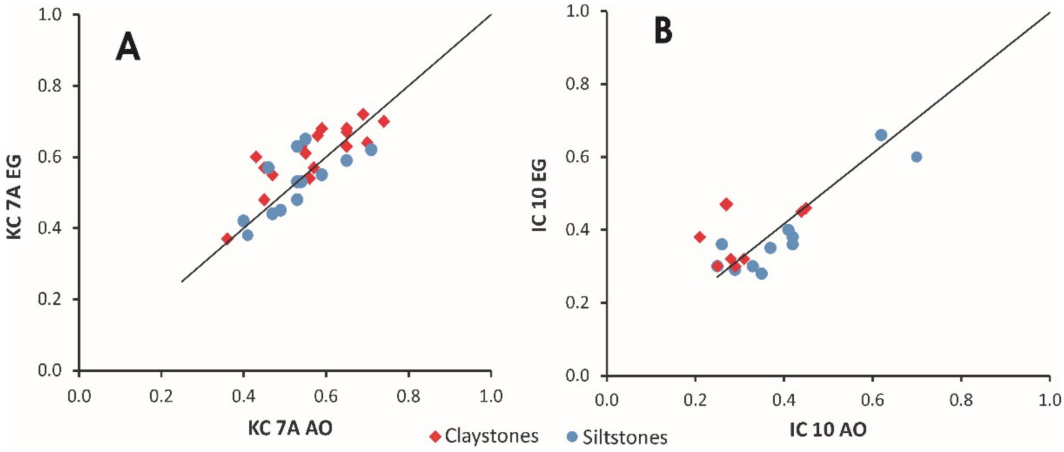

Figure 3. (**A**) Kln crystallinity measured in AO samples vs Kln crystallinity measured in EG samples. (**B**) Illite crystallinity measured in AO samples vs. illite crystallinity measured in EG samples, both in clays and silts.

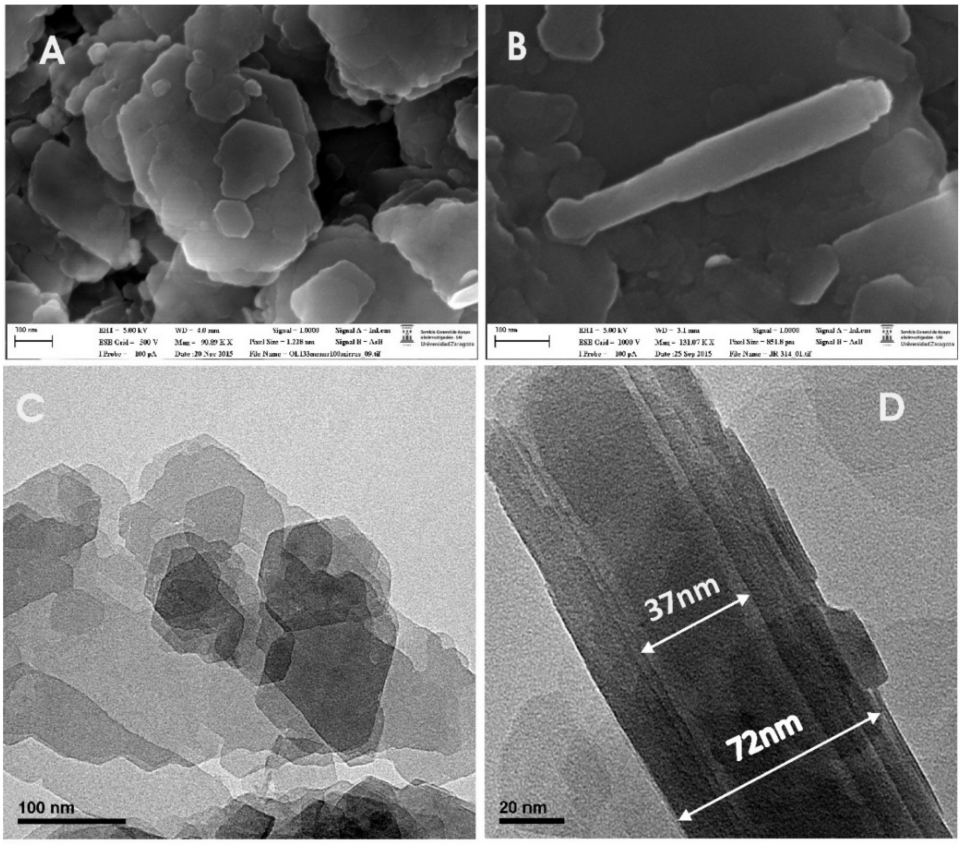

Figure 4. *Cont*.

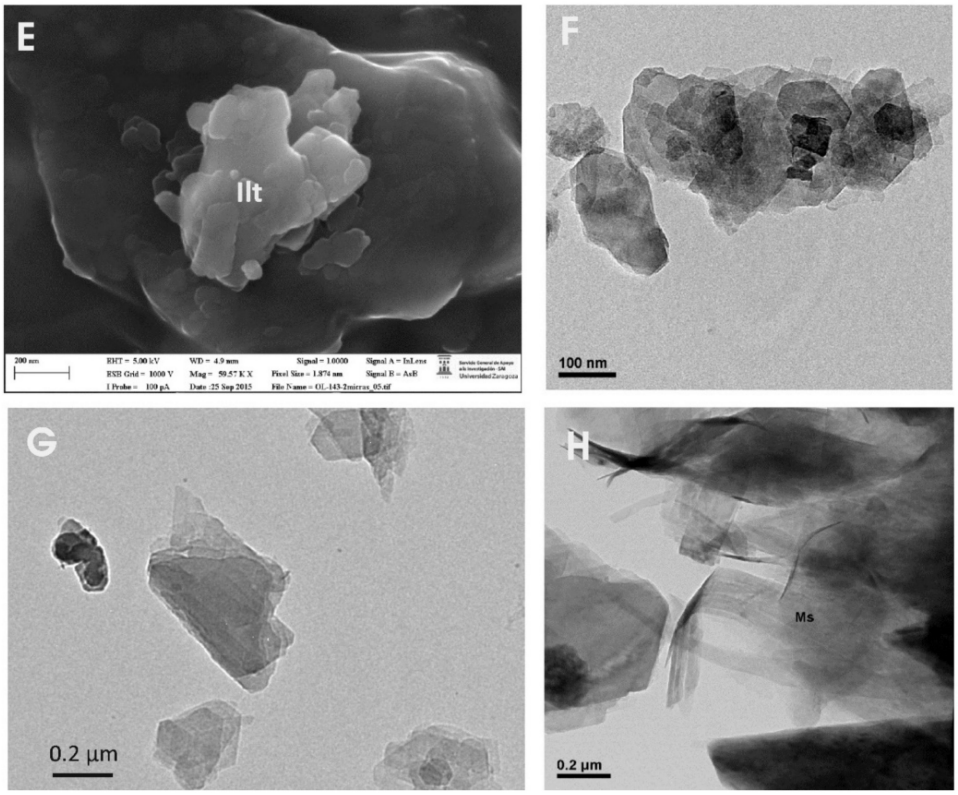

Figure 4. Electron microscopy images showing typical morphologies of kaolinites (**A**,**C**) and halloysites (**B**,**D**) and those of illites (**E**–**H**). (**A**,**B**,**E**) are FESEM/SE images; (**C**,**D**,**F**–**H**) are TEM images. Ilt = illite, Ms: muscovite.

In contrast, illites are present in the samples as anhedral to subhedral plates; these plates range fom micron to nanometer sizes (Figure 4E–G). In the case of the subhedral illite plates they sometimes have pseudohexagonal outlines (Figure 4F). Illites with lath morphologies and frayed edges are also observed (Figure 4H).

4.3. Microtexture and Composition of the Clays (FESEM/BSE Images)

BSE images of polished sections show that rock frameworks are formed by mixtures of detrital quartz, white K micas (muscovite), and accessory K feldspars, along with Fe and Ti oxides (Figure 5A,B). The large phyllosilicates have random orientations (Figure 5A). On the other hand, the matrix consists of fine mixtures of kaolinite and illite (or IS phases) (Figure 5A,B).

Kaolinite-mica intergrowths are abundant in these rocks (Figure 5C–H). All of them have in common that both kaolinite and mica are stacked parallel to each other and the aggregates are up to 10–15 µm thick along the c axis.

Figure 5C,D, which is an enlargement of Figure 5C, show that the kaolinite is mainly on the edges of the intergrowths, suggesting that the mica is being replaced by kaolinite. Similar textural relations between these two phyllosilicates are also observed in Figure 5H. In large mica-kaolinite intergrowths, the kaolinite grows between cleavage sheets of pre-existing detrital mica. This produces the displacement of the mica sheets (Figure 5G). Intergrowths formed mainly of kaolinite, constituting booklet-type aggregates with only some mica relicts are also observed (Figure 5E,F). These textural relations suggest a more advanced process than that observed in Figure 5D,H. In some cases, the continuity of the thin packets of muscovite is more diffuse, and they seem to disappear into a kaolinite matrix (Figure 5F). Similar aggregates of lower size are observed forming the matrix but, in this case, they are only made up of kaolinite plates (Figure 5B).

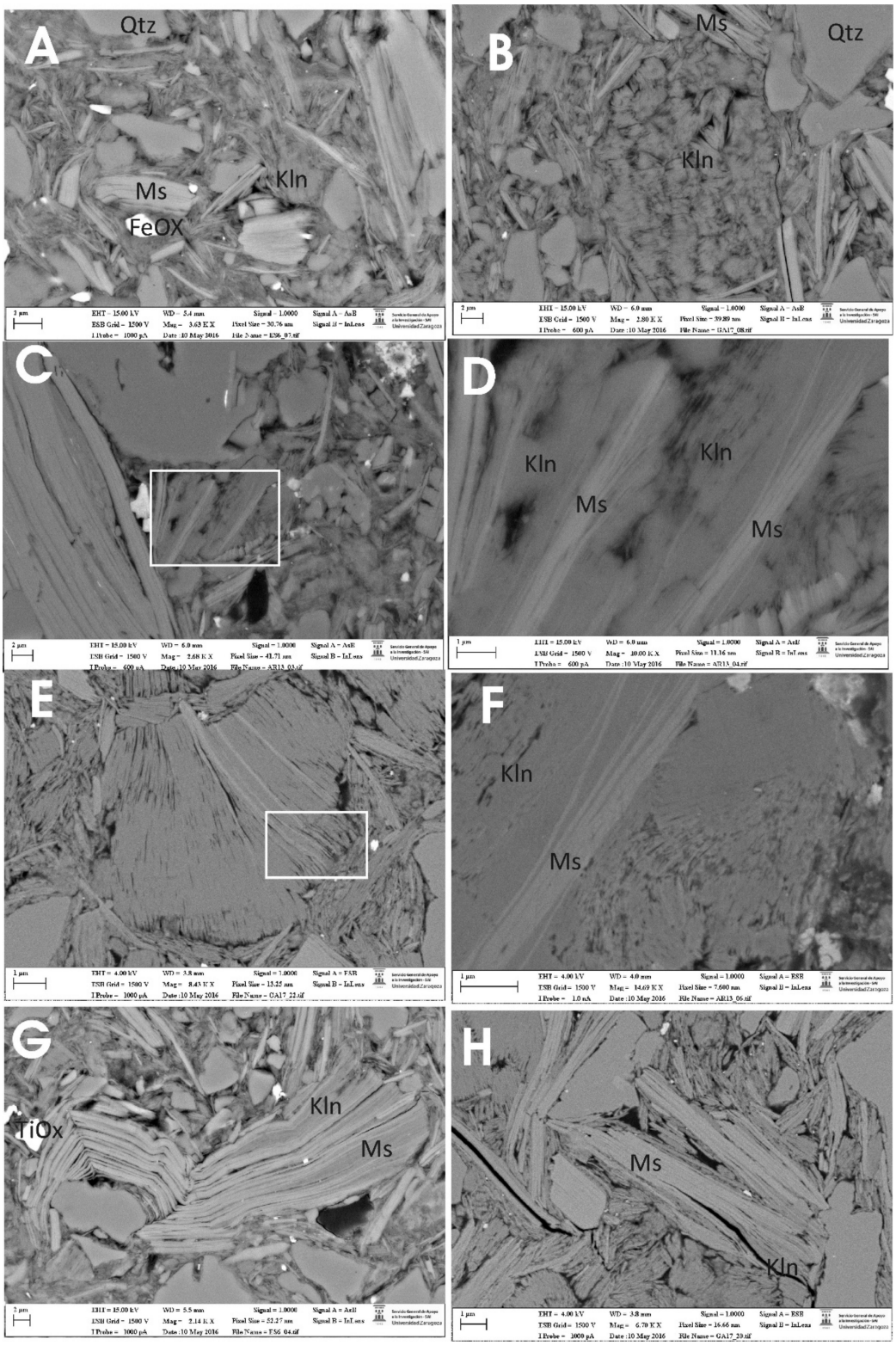

Figure 5. BSE/FESEM images of polished sections. (**A**,**B**) show the typical texture of the rocks with random orientations. (**C**–**H**) show the presence of mica-kaolinite intergrowths. (**D**) is an enlargement of (**C**). Qtz: Quartz, KF: K feldspar, M: Mica, Kln: kaolinite, FeOx: Fe oxides, TiOx: Ti oxides.

All these textures suggest an in-situ origin for kaolinites in contrast with the detrital origin of the K micas.

4.4. Nanotextures of the Clays (TEM Images)

TEM images show the textural elements depicted by FESEM: (1) Ms-Kln intergrowths and (2) the fine matrix formed by clays.

Figure 6 shows that these intergrowths are observed at the nanometric scale. In this figure, several mica-kaolinite intergrowths are illustrated. Both mica and kaolinite packets are of variable thickness, usually up to 10–15 Å.

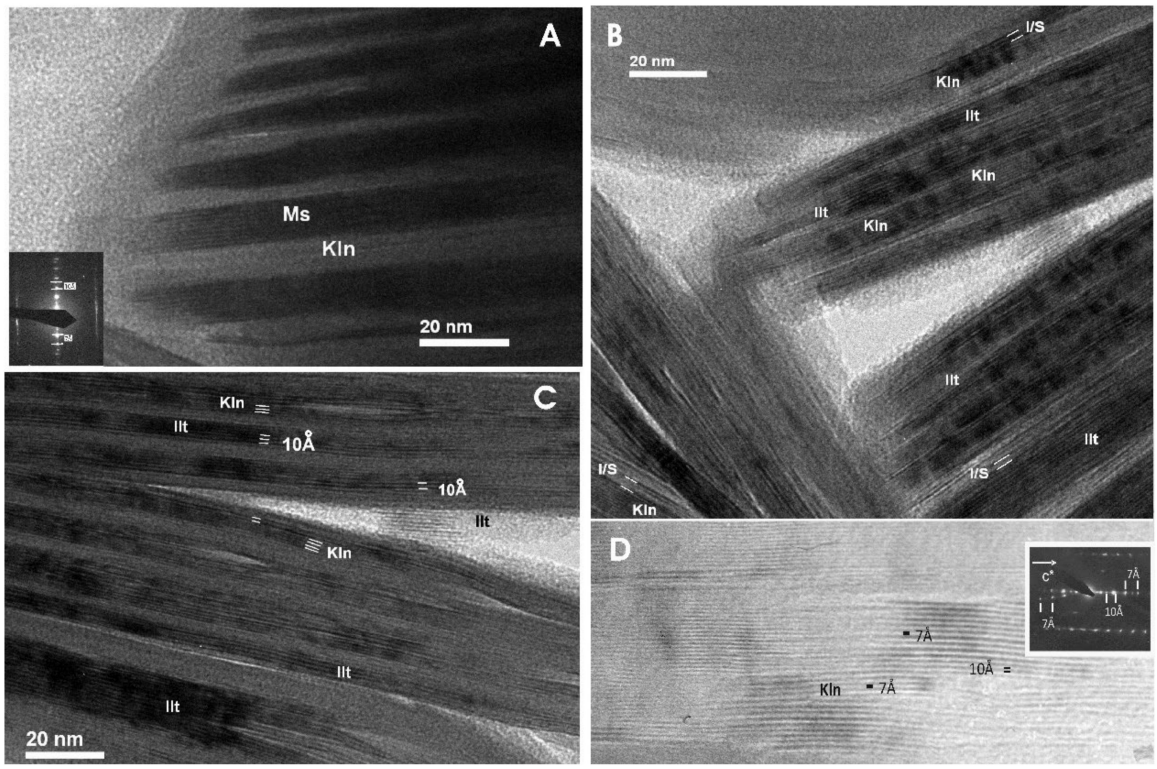

Figure 6. High Resolution TEM images and SAED patterns (insets of mica-kaolinite intergrowths (**A**–**C**) and 10 Å to 7 Å layer transitions (**D**).

Figure 6A corresponds to a >100 Å thick mica-kaolinite intergrowth. The mica packets are thinner towards the edge of the sample. SAED patterns (inset in Figure 6A) show how the c* crystallographic axes of both phases are parallel to each other, and the 00l reflections of both kaolinite and mica are also observed. Figure 6B shows much thinner intergrowths up to 30 nm thick, which consist of illite and kaolinite packets. On occasion, mixed-layered I-S minerals are identified. They are 21 Å thick, which corresponds to the sum of one illite layer (10 Å) plus one partially collapsed smectite layer (12 Å). These I/S units are in contact both with kaolinite and illite. In Figure 6C we observe similar intergrowths; here the mica layers are displaced because of the kaolinite growths, producing lenticular voids (v). Frayed illites are observed, like those shown among illite particles by TEM in Figure 4H. Evidence of 10 Å to 7 Å layer transitions is observed (Figure 6D), and the corresponding SAED patterns show that the c* axes of both clays are parallel to each other and to the 00l reflections of both phases.

In summary, HRTEM images show the existence of kaolinite-mica intergrowths at the nanometer scale as well as complex and disordered interlayering among kaolinite, muscovite, and IS phases.

High Resolution TEM (HRTEM) images of the fine-grained matrix show the presence of abundant illite, kaolinite, I-S phases, and smectite. Halloysite is not distinguished in these images, but it was observed in FESEM and TEM images of clay particles.

According to the HRTEM images, the clay matrix is quite heterogeneous. There are some areas with parallel to subparallel illite and kaolinite packets, with thicknesses ranging from 5 to 20 nm (Figure 7A). On occasion, kaolinite or illite form mixed layers with I-S

phases, and their lattice fringe images show abundant layer terminations. In other zones, as Figure 7B illustrates, there are frayed oblique illite packets that show disordered SAED suggesting a 1 Md polytype. Complex mixed-layered minerals formed by Sm-layers and IS phases are also observed in HRTEM images of the matrix (Figure 7C), and they also show disordered polytypes (1 Md type). In Figure 7D, a number of IS phases are interstratified with illite layers (10 Å spacing). Random mixed-layered illite/kaolinite are visualized in Figure 7E; the presence of layer terminations in the images and the SAED patterns indicate that they are defective structures. Pure kaolinite areas are also observed (Figure 7F). The layer terminations and non-straight lattices observed in the HRTEM images of kaolinite along with the disordered polytypes (SAED patterns) suggest that the kaolinite has low crystallinity.

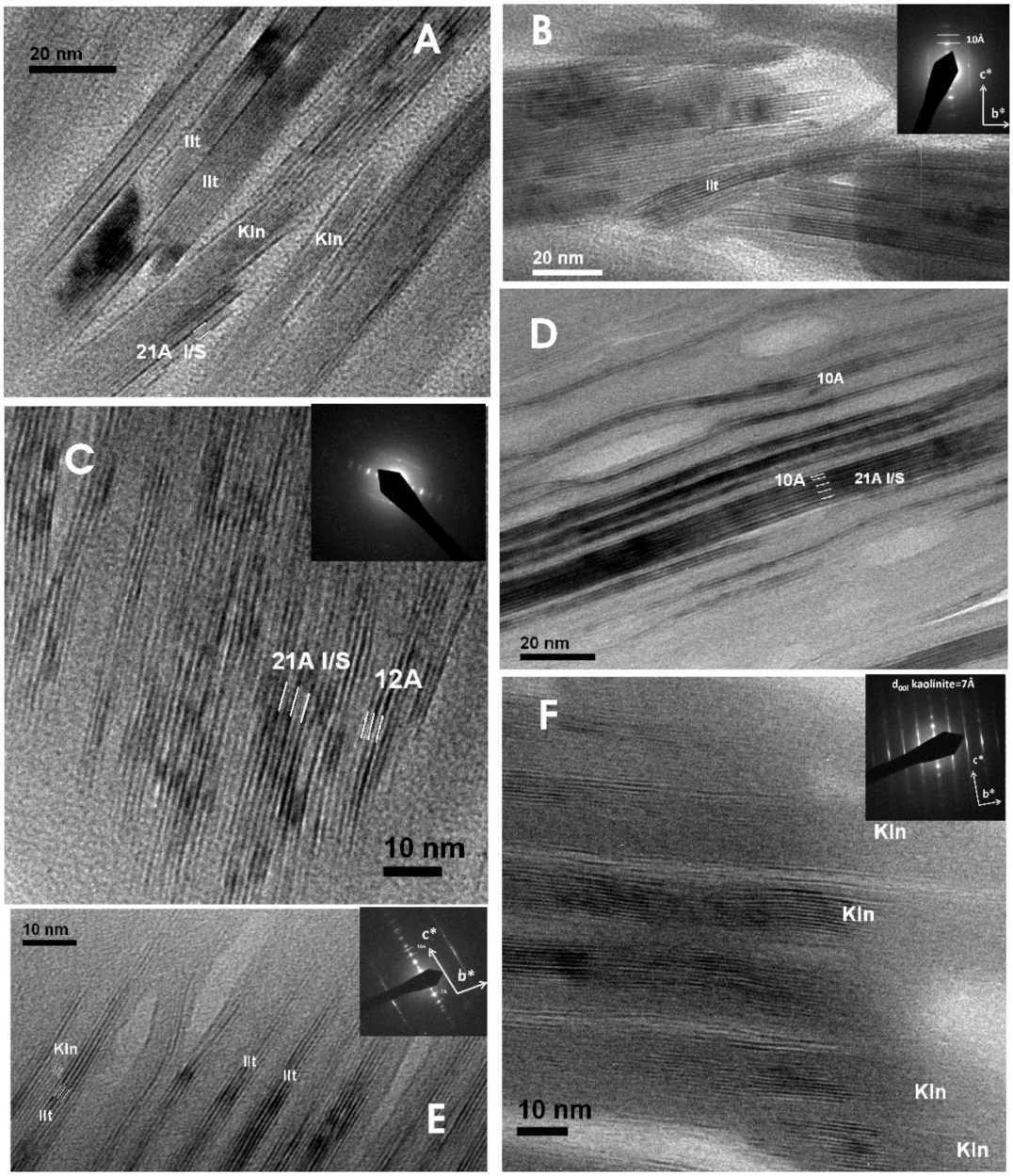

Figure 7. HRTEM images corresponding to the fine clay matrix of the rocks. (**A**) Clay matrix formed by illite (Ilt), kaolinite (kln) and I/S mixed layers. (**B**) Frayed oblique illite (Ilt) packets, inset shows disordered SAED suggesting a 1 Md polytype. (**C**) Complex mixed-layered minerals formed by Sm-layers and IS phases, inset shows disordered polytypes (1 Md type). (**D**) I-S phases interstratified with illite layers (10 Å spacing). (**E**) Random mixed-layered illite/kaolinite (Ilt/Kln). (**F**) Pure kaolinite areas with layer terminations and non-straight lattices, inset shows SAED pattern suggesting disordered polytypes.

In summary, high-resolution images corresponding to fine matrix show very complex relations between the three types of phases. We have observed defective illite and kaolinite, and random mixed layers of Kln-IS, Ilt-IS, and IS-S. In general, the SAED patterns suggest disordered polytypes.

4.5. Chemical Composition of the Studied Ball Clays

These clayey deposits are SiO_2- and Al_2O_3-rich, with average contents of 57.7% and 23.1%, respectively, with low Fe_2O_3 (3.5%) and K_2O (2.6%) and very low contents in S (0.2%), TiO_2 (0.9%), MgO (0.6%), Na_2O (0.4%), CaO (0.4%), P_2O_5 (0.10%), and MnO (0.03%). The mean value of the loss of ignition (LOI) is 10.2%, which results from the hydrated minerals (e.g., phyllosilicates) and the organic matter of the samples.

The studied ball clays are of a similar composition to other ball clays (Figure 8). The differences are related to the Al_2O_3 content, which is lower in the Iberian ball clays (23.1%) than in those from Devon (27.29%) and Poland (25.9%), and the higher Fe_2O_3 (3.5%) with respect to those from Devon (0.97%) and Poland (1.0%). Plots of the analyses of these groups of ball clays overlap each other in the Al_2O_3-SiO_2- (Fe_2O_3 + TiO_2 + Na_2O + CaO + K_2O) plot. In an enlargement of a part of the plot, we can observe that the SiO_2/Al_2O_3 variations are similar in each group and that the NE Spanish clays are slightly displaced towards the (Fe_2O_3 + TiO_2 + Na_2O + CaO + K_2O) vertex.

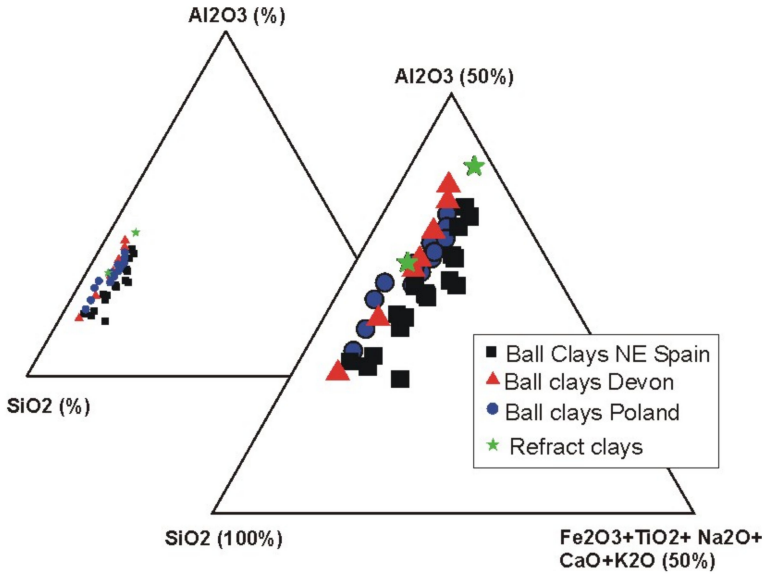

Figure 8. Plot of the chemical composition of the ball clays from NE Spain (this study), ball clays from Devon [1], ball clays from Poland [9], and refractory clays [24]. (Table S1).

5. Discussion

5.1. Mineralogy of the Ball Clay Deposits

The mineralogical composition of the levels analyzed by XRD and FESEM shows the coexistence of dioctahedral micas (muscovite and illites), kaolinite, quartz and minor feldspars, and Fe and Ti oxides. According to the bibliography, this is the characteristic mineralogy of ball clays. The mineral assemblages are quite homogenous throughout the formation. Only relative variations among the mineral phases are observed, reflecting the sampled lithologies.

The simplicity in the mineralogy contrasts with the electron-microscopy observations. The combination of FESEM and HRTEM shows the presence of complex mixtures of various types of dioctahedral phyllosilicates such as kaolinite, muscovite, illite, smectite, mixed-layered IS, along with non-clay phases such as quartz and minor feldspars, Ti and Fe oxides, and organic matter.

Some of the phyllosilicates are of micron size and are clearly visible at the SEM scale, such as muscovite and kaolinite. They form discrete phases, with intergrowths between them. Kaolinite also forms booklets up to 15 μm. The texture of the kaolinites in booklets and intergrowths with mica suggests that they are authigenic. In the latter, kaolinite growths displace mica sheets. The textures also show some kind of alteration from mica to kaolinite, as it has been confirmed by TEM with the observation of the illite- to kaolinite-layer transitions. TEM also shows the presence of I-S phases as minor components interlayered with illite and kaolinite.

The matrix of the rocks is mainly formed by illite and kaolinite, which show 5 to 20 nm thick packets, as the HRTEM images reflect. These sizes are too small to be resolved by FESEM. TEM analyses of clay particles reveal that the kaolinites usually have smaller crystal sizes than the illites. High-resolution images show that, in addition to kaolinite and illite in the matrix, there are also very complex interlayered phases such as Kln-IS, Ilt-IS, IS, and IS-Sm. These usually display random ordering. The random stacking produces SAED patterns typical of disordered polytypes.

The interstratifications of illite and kaolinite with expandable phases is reflected in the crystallinity indices determined by XRD. Figure 3 shows that some of the crystallinity index measurements have larger values in the EG-treated samples than in the air-dried samples, reflecting the presence of the same expandable components both in illites and kaolinites. These clays are disordered and have defective structures, as it has been inferred from HRTEM images and SAED patterns.

Therefore, although the XRD data show the presence of the major phases in the analyzed ball clays and the presence of some expandable components both in illite and kaolinite, the use of high-resolution electron images is essential to ascertain in detail the presence of complex intergrowths and interstratifications. The described mineralogical characteristics, along with the presence of organic matter, are responsible for the plasticity of these deposits.

5.2. Genesis of the Clay Minerals

Previous studies [12] suggest a detrital origin for all the clays in these deposits. However, the use of high-resolution techniques provides evidence of the coexistence of detrital and authigenic clays.

The euhedral to subhedral pseudohexagonal kaolinite plates and the occurrence of halloysite tubes suggest that they are probably of in-situ origin. The presence of kaolinite plates forming delicate book-like aggregates suggests that they would not have resisted sedimentary transport, and the growth of kaolinite among mica sheets and the alteration of mica to kaolinite support the hypothesis of an authigenic origin of the kaolinite. In contrast, the anhedral morphology of the illites and the evidence of illite alteration (e.g., frayed illites) suggest a detrital origin for the illites.

Further evidence of mica alteration would be the presence of expandable phases interstratified with illite. In the case of interstratifications with kaolinites, the expandable phases may be the reaction product of the alteration of K micas, which are more easily altered than kaolinites.

Experimental studies [25] have established that in pH $\leq$ 3 and low ionic-strength experiments, illite alteration takes place with the removal of interlayer K followed by the dissolution of octahedral cations (Fe, Mg, and Al), the dissolution of Si being the limiting step in the illite dissolution processes. These authors established that the dissolution rate of illite was mainly controlled by the solution pH and no effect of ionic strength was observed on the dissolution rates. Other authors [26] indicate that at acidic pH the reaction rate appears to be controlled by the breaking of tetrahedral Si-O bonds after adjoining tetrahedral Al has been removed by the proton exchange reaction.

The sedimentary environment of the analyzed ball clays provides specific conditions favoring the alteration or destabilization of illite. As it has been described in the Geological Information section, the studied ball clay deposits are part of continental sedimentary

deposits formed in transitional environments. Specifically, the Escucha Formation in this area corresponds to a mudflat environment with freshwater swamp plains. At the beginning of the lower Albian, the sedimentation in these areas was typical of a coastal marine environment, but it then evolved into a mudflat environment with freshwater swamp plains. The accumulation of these clay deposits along with subbituminous coal deposits was favored by several factors, including the paleogeography, which enhanced the occurrence of these materials in areas of high subsidence (e.g., the Ariño-Estercuel, Utrillas-Aliaga, Castellón, and Calanda subbasins). Tectonics and stratigraphy were also controlling factors, since tectonics fragmented the upper Aptian platform and created the sedimentary basins where the Escucha Formation was deposited, and the coal and kaolinite-rich levels were well developed when these appropriate continental characteristics prevailed [13].

The presence of abundant organic matter both in the coal and the clay deposits suggests the presence of organic- and acidic-rich fluids that would have been responsible for silicate alteration (micas, feldspars) and the subsequent formation of kaolinite, as other authors have suggested [27–33]. The complex intergrowths and interlayering observed both at micron- and nano-scale suggest that the mineral reactions (dissolution and alteration of K silicates) were not complete.

Some authors suggest that kaolinite can also form under early diagenetic (reducing) conditions [34,35], reporting kaolinite formation by weathering in paleosols and by the early diagenesis of dark grey mudstone facies under the meteoric water table. In the studied case, crystallization of kaolinite probably started under sedimentary conditions, and it may have progressed under early diagenetic conditions. The presence of the subbituminous coal levels interbedded with the clay deposits suggests a low degree of diagenesis, reaching temperatures probably lower than 100 °C. This suggests that these deposits underwent only a very low degree of diagenetic evolution.

6. Conclusions

The combination of XRD, FESEM, and TEM techniques indicates that the analyzed ball clays consist of complex intergrowths at the micron scale, and complex, disordered mixed-layered phases at nanometer scale formed by kaolinite, micas, illite, illite-smectite phases, and smectite. Detrital micas and illites were altered and replaced by illite-smectite, kaolinite, and smectite. The kaolinite textures also indicate an in-situ origin for this mineral that grows on micas and fills pores. The textures of the rocks along with the organic matter content generate the plasticity.

The authigenesis of kaolinite and the alteration of detrital clays took place under sedimentary conditions and were favored by the presence of freshwater swamp plains, acidic conditions, and the paleogeography.

Supplementary Materials: The following are available online at https://www.mdpi.com/article/10.3390/min11121339/s1, Figure S1: XRD patterns of oriented kaolinite- rich fractions (<2 μm fractions, air-dried oriented samples) corresponding to (a) a siltstone, (b) a claystone. Table S1: Chemical compositions (wt %) of ball clays from NE Spain (this study), ball clays from Devon [1], ball clays from Poland [9], and refractory clays [24].

Author Contributions: B.B.: Fieldwork and sampling, FESEM and TEM study, funding acquisition and writing-review. M.J.M.: Fieldwork and sampling, XRD study and review. E.L.: XRD study and review. A.Y.: Fieldwork, XRD and sampling and review. All authors have read and agreed to the published version of the manuscript.

Funding: This research was funded by the Spanish Ministry of Science, Innovation and Universities [grant number RTI2018-093419-B-100 and the European Regional Development Fund and the Government of Aragon [Aragosaurus Group: Geological Resources and Palaeoenvironments, grant number E18_20R].

Acknowledgments: The authors are grateful to the journal reviewers, for their helpful comments and suggestions. They would like to acknowledge the use of the Servicio General de Apoyo a la

Investigación-SAI, University of Zaragoza. They also thank to Cristina Gallego and Maria Angeles Laguna for their advice during the FESEM and TEM sessions.

Conflicts of Interest: The authors declare no conflict of interest.

References

1. Wilson, I.R. The constitution, evaluation and ceramic properties of ball clays. *Ceramica* **1998**, *44*, 287–288. [CrossRef]
2. Dondi, M.; Guarini, G.; Raimondo, M.; Salucci, F. Influence of mineralogy and particle size on the technological properties of ball clays for porcelain stoneware tiles. *Tile Brick Int.* **2003**, *20*, 2–11.
3. Andreola, F.; Siligardi, C.; Manfredini, T.; Carbonchi, C. Rheological behaviour and mechanical properties of porcelain stoneware bodies containing Italian clay added with bentonites. *Ceram. Int.* **2009**, *36*, 1159–1164. [CrossRef]
4. De Noni, A., Jr.; Hotza, D.; Cantavella Soler, V.; Sanchez Vilches, E. Analysis of the development of microscopic residual stresses on quartz particles in porcelain tile. *J. Eur. Ceram. Soc.* **2008**, *28*, 2629–2637. [CrossRef]
5. Ferrari, S.; Gualtieri, A.F. The use of illitic clays in the production of stoneware tile ceramics. *Appl. Clay Sci.* **2006**, *32*, 73–81. [CrossRef]
6. Leonelli, C.; Bondioli, F.; Veronesi, P.; Romagnoli, M.; Manfredini, T.; Pellacani, G.C.; Canillo, V. Enhancing the mechanical properties of porcelain stoneware tiles: A microstructural approach. *J. Eur. Ceram. Soc.* **2001**, *21*, 785–793. [CrossRef]
7. Baioumy, H.M.; Ismael, I.S. Composition, origin and industrial suitability of the Aswan ball clays, Egypt. *Appl. Clay Sci.* **2014**, *102*, 202–212. [CrossRef]
8. Dondi, M.; Raimondo, M.; Zanelli, C. Clays and bodies for ceramic tiles: Reappraisal and technological classification. *Appl. Clay Sci.* **2014**, *96*, 91–109. [CrossRef]
9. Galos, K. Composition and ceramic properties of ball clays for porcelain stoneware tiles manufacture in Poland. *Appl. Clay Sci.* **2011**, *51*, 74–85. [CrossRef]
10. Galos, K. Influence of mineralogical composition of applied ball clays on properties of porcelain tiles. *Ceram. Int.* **2011**, *37*, 851–861. [CrossRef]
11. Jordán, M.M.; Meseguer, S.; Pardo, F.; Montero, M.A. Properties and possible ceramic uses of clays from lignite mine spoils of NW Spain. *Appl. Clay Sci.* **2015**, *118*, 158–161. [CrossRef]
12. Bauluz, B.; Mayayo, M.J.; Yuste, A.; González López, J.M. Genesis of kaolinite from Albian sedimentary deposits of the Iberian Range (NE Spain): Analysis by XRD, SEM and TEM. *Clay Miner.* **2008**, *43*, 459–475. [CrossRef]
13. Querol, X.; Salas, R.; Pardo, G.; Ardevol, L. Albian coal-bearing deposits of the Iberian Range in north eastern Spain. In *Controls on the Distribution and Quality of Cretaceous Coals*; McCabe, P.J., Totman, J.P., Eds.; Geological Special Paper 267; Geological Society of America: Boulder, CO, USA, 1992; pp. 193–208.
14. Schultz, L.G. Quantitative interpretation of mineralogical composition from X-ray and chemical data for the Pierre shale. *Prof. Pap. Geol. Surv.* **1964**, *391-c*, 31.
15. Biscaye, P.E. Mineralogy and sedimentation of recent deep-sea clay in the Atlantic Ocean and adjacent seas and ocean. *Geol. Soc. Am. Bull.* **1965**, *76*, 803–832. [CrossRef]
16. Martin, J.D. A software package for powder x-ray diffraction analysis. *Qual. Quant. Microtexture* **2017**, *5*, 121.
17. Churchman, G.J.; Theng, B.K.G. Interactions of halloysites with amides: Mineralogical factors affecting complex formation. *Clay Miner.* **1984**, *19*, 161–175. [CrossRef]
18. Kim, J.W.; Peacor, D.R.; Tessier, D.; Elsass, F. A technique for maintaining texture and permanent expansion of smectite interlayers for TEM observations. *Clays Clay Miner.* **1995**, *43*, 51–57. [CrossRef]
19. Sánchez-Roa, S.; Bauluz, B.; Nieto, F.; Abad, I.; Jimenéz-Millán, J.; Faulkner, D. Micro- and nano-scale study of deformation induced mineral transformations in Mg-phyllosilicate-rich fault gouges from the Galera Fault Zone (Betic Cordillera, SE Spain). *Am. Mineral. J. Earth Planet. Mater.* **2018**, *103*, 1604–1631. [CrossRef]
20. Guthrie, G.D.; Veblen, D.R. High-resolution transmission electron microscopy of mixed-layer illite/Smectite: Computer simulation. *Clays Clay Miner.* **1989**, *37*, 1–11. [CrossRef]
21. Guthrie, G.D.; Veblen, D.R. High-resolution Transmission electron microscopy applied to clay minerals. In *Spectroscopic Characterization of Minerals and Their Surfaces*; Coyne, L.M., Mckeever, S.W.W., Blake, D.F., Eds.; Symposia Series 415; American Chemical Society: Washington, DC, USA, 1989; pp. 75–93.
22. Guthrie, G.D.; Veblen, D.R. Interpreting one-dimensional High-resolution transmission electron micrographs of sheet silicates by computer simulation. *Am. Mineral.* **1990**, *75*, 276–288.
23. Bauluz, B.; Peacor, D.R.; Gonzalez-Lopez, J.M. Transmission electron microscopy study of illitization in pelites from the Iberian Range, Spain: Layer-by-layer replacement? *Clays Clay Miner.* **2000**, *48*, 374–384. [CrossRef]
24. Djangang, C.N.; Elimbi, A.; Melo, U.C.; Lecomte, G.L.; Nkoumbou, C.; Soro, J.; Yvon, J.; Blanchart, P.; Njopwouo, D. Refractory ceramics from clays of Mayouom and Mvan in Cameroon. *Appl. Clay Sci.* **2008**, *39*, 10–18. [CrossRef]
25. Bibi, I.; Singh, B.; Silvester, E. Dissolution of illite in saline-acidic solutions at 25 °C. *Geochim. Cosmochim. Acta* **2011**, *75*, 33237–33249. [CrossRef]
26. Oelkers, E.H.; Schott, J.; Gauthier, J.M.; Roncal-Herrero, J. An experimental study of the dissolution mechanism and rates of muscovite. *Geochim. Cosmochim. Acta* **2008**, *72*, 4948–4961. [CrossRef]

27. Rossel, N.C. Clay mineral diagenesis in Roetliegend aeolian sandstones of the southern North Sea. *Clay Miner.* **1992**, *17*, 69–77. [CrossRef]
28. Blackbourn, G.A. Diagenetic history and reservoir quality of a Brent sand sequence. *Clay Miner.* **1984**, *19*, 377–389. [CrossRef]
29. Goodchild, M.W.; Whitaker, J.C.M. A graphic study of the Rotliegendes sandstone reservoir North Sea. *Clay Miner.* **1986**, *21*, 459–477. [CrossRef]
30. Pye, K.; Krinsley, D.H. Diagenetic carbonate and evaporite minerals in Rotliegend aeolian sandstones of the southern North Sea: Their nature and relationship to secondary porosity development. *Clay Miner.* **1986**, *21*, 443–457. [CrossRef]
31. Ehrenberg, S.N. Kaolinized, potassium-leached zones at the contacts of the Garn formation, Haltenbanken, mid-Norwegian continental shelf. *Mar. Pet. Geol.* **1991**, *8*, 250–269. [CrossRef]
32. Gaupp, R.; Matter, A.; Platt, J.; Ramseyer, K.; Walzebuck, J. Diagenesis and fluid evolution of a deeply buried Permian (Rotliegende) gas reservoir, Northwest Germany. *AAPG Bull.* **1993**, *77*, 1111–1128.
33. Platt, J.D. Controls on clay mineral distribution and chemistry in the early Permian Rotliegend of Germany. *Clay Miner.* **1993**, *28*, 393–416. [CrossRef]
34. Pe-Piper, G.; Dolansky, L.; Piper, D.J.W. Sedimentary environment and diagenesis of the Lower Cretaceous Chaswood Formation, southeastern Canada: The origin of kaolin-rich mudstones. *Sediment. Geol.* **2005**, *178*, 75–97. [CrossRef]
35. Piper, D.J.W.; Hundert, T.; Pe-Piper, G.; Okwese, A.C. The roles of pedogenesis and diagenesis in clay mineral assemblages: Lower Cretaceous fluvial mudrocks, Nova Scotia, Canada. *Sediment. Geol.* **2009**, *213*, 51–63. [CrossRef]